

# **Systematic Climate Model Rainfall Biases over Southern Africa: Links to Moisture Circulation and Topography**

C. MUNDAY AND R. WASHINGTON

*School of Geography and Environment, University of Oxford, Oxford, United Kingdom*

(Manuscript received 9 January 2018, in final form 14 June 2018)

## ABSTRACT

An important challenge for climate science is to understand the regional circulation and rainfall response to global warming. Unfortunately, the climate models used to project future changes struggle to represent present-day rainfall and circulation, especially at a regional scale. This is the case in southern Africa, where models from phase 5 of the Coupled Model Intercomparison Project (CMIP5) overestimate summer rainfall by as much as 300% compared to observations and tend to underestimate rainfall in Madagascar and the southwest Indian Ocean. In this paper, we explore the climate processes associated with the rainfall bias, with the aim of assessing the reliability of the CMIP5 ensemble and highlighting important areas for model development. We find that the high precipitation rates in models that are wet over southern Africa are associated with an anomalous northeasterly moisture transport ( $\sim 10\text{--}30\text{ g kg}^{-1}\text{ s}^{-1}$ ) that penetrates across the high topography of Tanzania and Malawi and into subtropical southern Africa. This transport occurs in preference to a southeasterly recurvature toward Madagascar that is seen in drier models and reanalysis data. We demonstrate that topographically related model biases in low-level flow are important for explaining the intermodel spread in rainfall; wetter models have a reduced tendency to block the oncoming northeasterly flow compared to dry models. The differences in low-level flow among models are related to upstream wind speed and model representation of topography, both of which should be foci for model development.

## 1. Introduction


The future evolution of the climate system under unprecedented human forcing is uncertain. Climate models are our only tools for projecting future climate change, and yet they contain large errors relative to observations, particularly for societally important variables such as rainfall (Biasutti 2013; Mehran et al. 2014; Yang et al. 2015; Lintner et al. 2017; James et al. 2018). Understanding the climate processes that underlie climate model errors is a first step toward assessing models' reliability for projecting future change, and can also help to guide future model development. This is particularly important in cases where an ensemble of models displays a


systematic bias compared to observations. A wide spread of model simulations around observations might be indicative of random error that will cancel in a multimodel mean (MMM), whereas a consistent direction of error implies some common structural error that will not cancel in an MMM (Sanderson and Knutti 2012).

In subtropical southern Africa ( $20^{\circ}\text{--}30^{\circ}\text{E}$ ,  $20^{\circ}\text{--}30^{\circ}\text{S}$ ), climate models from the most recent phase (phase 5) of the Coupled Model Intercomparison Project (CMIP5; Taylor et al. 2012) systematically overestimate climatological summer rainfall (Fig. 1a). Some models simulate 3 times more rainfall than satellite/rain gauge observations.

*Publisher's Note:* This article was revised on 19 September 2018 to add the open access and CC BY designations that were missing when originally published.

*Publisher's Note:* This article was revised on 25 October 2018 to replace an incorrect version of Fig. 4 that was mistakenly used when originally published.

 Denotes content that is immediately available upon publication as open access.

 Supplemental information related to this paper is available at the Journals Online website: <https://doi.org/10.1175/JCLI-D-18-0008.s1>.

*Corresponding author:* Callum Munday, [callum.munday@ouce.ox.ac.uk](mailto:callum.munday@ouce.ox.ac.uk)



This article is licensed under a [Creative Commons Attribution 4.0 license](http://creativecommons.org/licenses/by/4.0/) (<http://creativecommons.org/licenses/by/4.0/>).

DOI: 10.1175/JCLI-D-18-0008.1

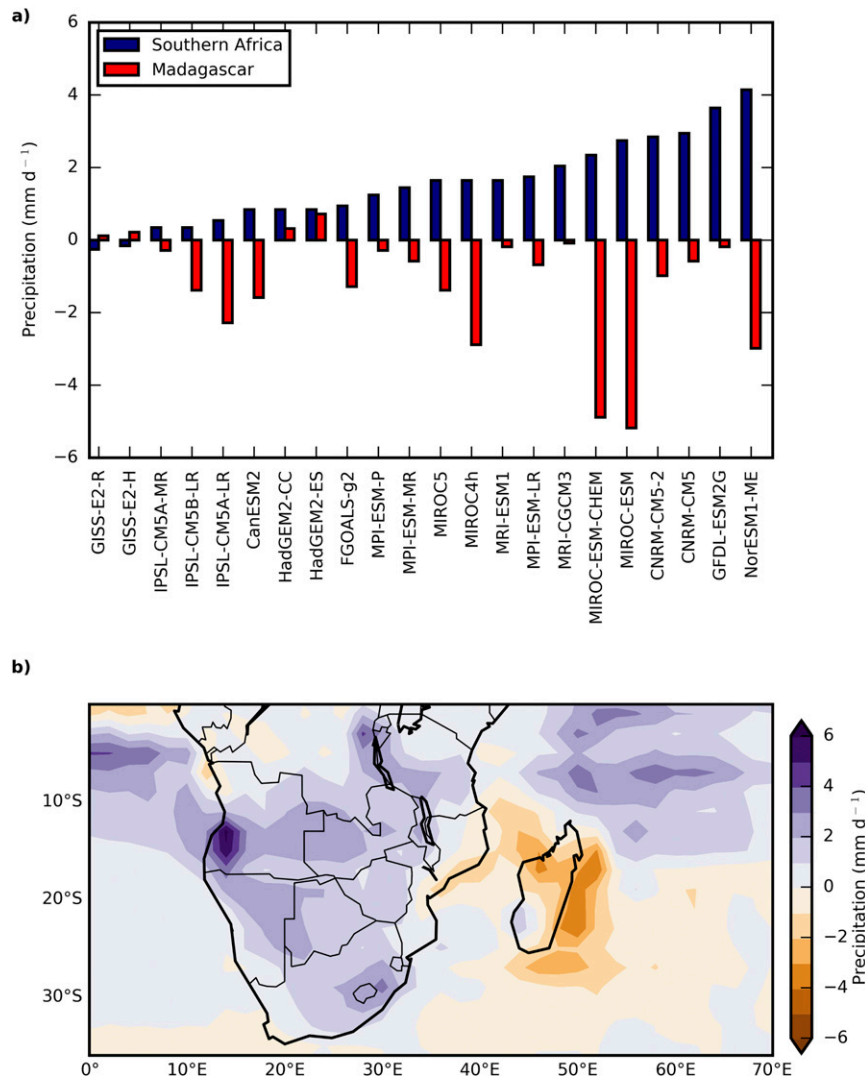


FIG. 1. (a) JF climatological rainfall bias (1979–2005) in CMIP5 models relative to CMAP satellite-rain gauge product in subtropical southern Africa ( $20^{\circ}$ – $30^{\circ}$ E,  $20^{\circ}$ – $30^{\circ}$ S; blue bars) and in Madagascar ( $44^{\circ}$ – $56^{\circ}$ E,  $12^{\circ}$ – $28^{\circ}$ S; red bars). (b) JF multimodel mean precipitation bias (1979–2005) relative to CMAP.

The large and systematic rainfall bias drives excessive evapotranspiration ( $\sim +0.5 \text{ mm day}^{-1}$ ) and cool temperature anomalies compared to observations (Mueller and Seneviratne 2014). The excessive rainfall is associated with a large off-equatorial diabatic heat source, and is therefore likely to influence the strength and character of regional overturning circulations (Chan and Nigam 2009). The problem has persisted through coupled model generations from CMIP3 (Christensen et al. 2007; Moise and Hudson 2008) to CMIP5 (Fig. 1; Dieppois et al. 2015) and is also present in atmosphere-only models (Goddard and Graham 1999; Cook 2000; Lazenby et al. 2016).

The rainfall bias in the multimodel mean has a dipole structure with excessive rainfall over southern Africa

(+40%) and a rainfall deficit over Madagascar and the southwestern Indian Ocean ( $-30\%$ ; Fig. 1b). The dipole is a feature of 20 out of 22 models used in this study (Fig. 1a), including two models that have a dipole of the opposite sign, with diminished southern African rainfall and enhanced Madagascan rainfall. This raises the question of whether there is a common process error in models that encourages rainfall in southern Africa at the expense of rainfall over Madagascar. In this paper we aim to define this process.

## 2. Data

We estimate rainfall from the Climate Prediction Center Merged Analysis of Precipitation (CMAP; Xie

TABLE 1. CMIP5 models. Models are ordered from dry to wet according to mean JF precipitation ( $20^{\circ}$ – $30^{\circ}$ E,  $20^{\circ}$ – $30^{\circ}$ S). (Expansions of acronyms are available online at <http://www.ametsoc.org/PubsAcronymList>.)

Model	Modeling group
GISS-E2-R	Goddard Institute for Space Studies
GISS-E2-H	Goddard Institute for Space Studies
IPSL-CM5A-MR	L'Institut Pierre-Simon Laplace
IPSL-CM5B-LR	L'Institut Pierre-Simon Laplace
IPSL-CM5A-LR	L'Institut Pierre-Simon Laplace
CanESM2	Canadian Centre for Modeling and Analysis
HadGEM2-CC	Met Office Hadley Centre
HadGEM2-ES	Met Office Hadley Centre
FGOALS-g2	State Key Laboratory Numerical Modeling for Atmospheric Sciences and Geophysical Fluid Dynamics
MPI-ESM-P	Max Planck Institute for Meteorology
MPI-ESM-MR	Max Planck Institute for Meteorology
MIROC5	National Institute for Environmental Studies (Japan), Atmosphere and Ocean Research Institute (University of Tokyo), Japan Agency for Marine-Earth Science and Technology
MIROC4h	See MIROC5
MRI-ESM1	Meteorological Research Institute
MPI-ESM-LR	Max Planck Institute for Meteorology
MRI-CGCM3	Meteorological Research Institute
MIROC-ESM-CHEM	See MIROC5
MIROC-ESM	See MIROC5
CNRM-CM5.2	Centre National de Recherches Météorologiques
CNRM-CM5	Centre National de Recherches Météorologiques
GFDL-ESM2G	Geophysical Fluid Dynamics Laboratory
NorESM1-ME	Norwegian Climate Centre

and Arkin 1997), a satellite-rain gauge product, which has similar rainfall climatology (1979–2005) to other satellite products over southern Africa (Novella and Thiaw 2013). There are some significant differences between reanalyses products in their estimation of southern African circulation (Zhang et al. 2013). Here we use data from two reanalyses products, NCEP2 (Kanamitsu et al. 2002) and ERA-Interim (Dee et al. 2011), to sample some of the uncertainty in the observed circulation. To get a different perspective on model performance in the subtropics we also use radiosonde data from Upington ( $28^{\circ}$ S,  $21^{\circ}$ E), which span 1976–1998 and 2008–2017. To estimate the climatology we use data from 1979 to 1994 when the data record is 89% complete for 0200 local time (LT) soundings and 61% complete for 1400 LT soundings.

Climate model data are from CMIP5 (Taylor et al. 2012). Topography data were only available for 23 models, and one model did not have specific humidity fields available. Therefore we evaluate 22 models (Table 1), using data from the first ensemble member for each model. All satellite, reanalysis, and model data are in the form of the climatological mean from 1979–2005 for January–February (JF), the core of the austral summer season, and are remapped to a common  $2^{\circ} \times 2^{\circ}$  grid. Locations referred to in the text are included in a political map of southern Africa (see Fig. S1 in the online supplemental material).

### 3. Background

We hypothesize that the wetter than observed model climatology in southern Africa is linked to the drier than observed model climatology in Madagascar through a common mechanism. To understand why this might be the case, we briefly review the circulation associated with the observed summer rainfall climatology and its variability.

#### a. The observed rainfall climatology

The latitude of maximum African tropical rainfall is equatorward of the maximum in solar insolation throughout the year. In the austral summer, a broad region of enhanced rainfall oriented northwest to southeast is present between  $8^{\circ}$  and  $22^{\circ}$ S over southern Africa and Madagascar (Fig. 2a). The land-based rainfall is not contiguous: there is one local maximum over northern Zambia ( $\sim 6$ – $8 \text{ mm day}^{-1}$ ) and another over Madagascar ( $\sim 12$ – $14 \text{ mm day}^{-1}$ ). The Madagascar rainfall maximum is the most poleward extension of the tropical rainband in the Southern Hemisphere. The broad pattern in the rainfall climatology is similar between CMAP and other rainfall datasets, although there are significant quantitative differences (Awange et al. 2015; Maidment et al. 2015). The drivers of the Madagascar rainfall maximum have not been fully demonstrated, with a combination of orographic

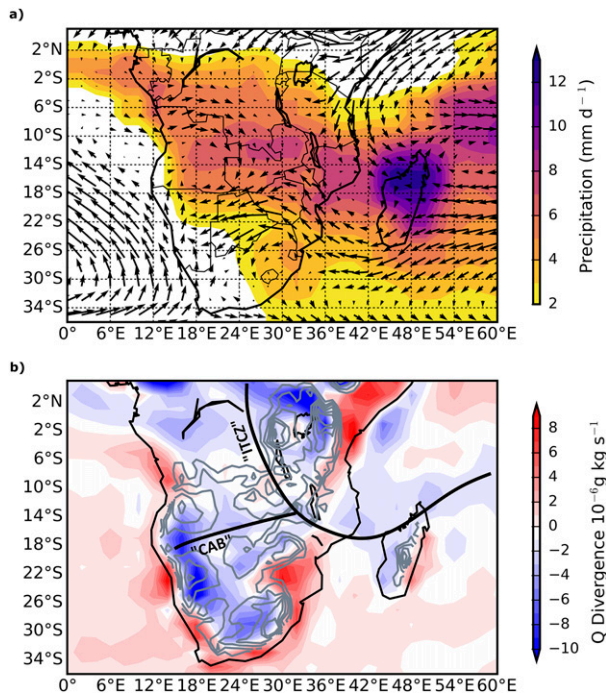


FIG. 2. (a) CMAP climatological precipitation (shaded) and (b) ERA-Interim reanalysis 850-hPa moisture flux climatology for JF (1979–2005). Gray contours show topography above 800 m (contour interval is 200 m) and moisture divergence ( $\text{g kg}^{-1} \text{s}^{-1} \times 10^6$ ) is shaded. The supposed positions of the CAB and ITCZ are drawn following van Heerden and Taljaard (1998).

forcing by the  $\sim 1500\text{-m}$ -high topography and the warm sea surface temperatures of the southwest Indian Ocean and Mozambique Channel likely to play a role.

Reference to the peak austral summer low-level (850 hPa) moisture circulation suggests that the processes controlling the maxima over the tropical subcontinent and over Madagascar are different (Fig. 2a). In northern Zambia most of the moisture supply originates from the equatorial Congo basin and flows cyclonically around a regional low pressure system: the Angola low. Some of this tropical northwesterly flow converges with subtropical southeasterlies, at the Congo Air Boundary (CAB; van Heerden and Taljaard 1998; Hachigonta and Reason 2006), although this convergence occurs predominantly to the south of the rainfall maximum (Fig. 2b). The Katanga plateau in southern Democratic Republic of Congo (DRC) and the Muchinga mountain range in northeastern Zambia are more closely located with the rainfall maximum. A number of large inland waterbodies, including Lake Malawi, Lake Tanganyika, and perhaps even Lake Kariba, could also influence the rainfall distribution.

The location of the ITCZ is often invoked as an explanation for the seasonal cycle in rainfall distribution

over Africa. In Fig. 2b, we have drawn on the canonical position of the ITCZ along the eastern Congo basin from Taljaard (1972) and van Heerden and Taljaard (1998). According to ERA-Interim data, the band of low-level convergence along the ITCZ is not continuous, with mean low-level divergence to the west and southwest of Lake Tanganyika. Counterintuitively, this area of low-level divergence is fairly closely located with the rainfall maximum, whereas the maximum in low-level convergence occurs to the northeast of the locus of tropical convection in the highlands of Tanzania, Kenya, and Uganda. In agreement with a recent review by Nicholson (2018), we view this as evidence that the concept of the ITCZ may not be useful for explaining the rainfall distribution over continental Africa.

Cross-equatorial northeasterlies are an important moisture source for subtropical southern Africa during wet years (D'Abreton and Tyson 1995; Washington and Preston 2006). In mean climatology, based on reanalyses with resolved topography reaching  $\sim 1200\text{ m}$ , only a small proportion of the northeasterlies penetrate across the high topography of northern Malawi and southern Tanzania (which, in reality, reaches a maximum of  $\sim 3000\text{ m}$  in the Kipengere range northeast of Lake Malawi). Instead, most of the northeasterly flow curves to the southeast in the vicinity of this topography toward the convection over Madagascar. The recurved flow converges with Indian Ocean easterlies in northern Madagascar, coinciding with the region of maximum summer rainfall.

The diminishing northeasterly flow with increasing latitude in subtropical southern Africa helps to set up a strong northeast to southwest rainfall gradient across the Kalahari basin (Tyson and Crimp 1998). Rainfall across this gradient decreases from  $\sim 7\text{ mm day}^{-1}$  in northern Zimbabwe to less than  $2\text{ mm day}^{-1}$  in southern Botswana, western South Africa, and Namibia. The reduced moisture supply and high average surface temperatures ( $>25^\circ\text{C}$ ) result in low relative humidity, which favors the formation of a thermal low over the western Kalahari in austral summer (Manatsa and Reason 2017). The thermal low is overlain by the Botswana (midlevel) high (Reason 2016). These conditions are clearly not present in some models (Fig. 1; Munday and Washington 2017).

#### b. The relationship between Madagascar and southern African rainfall

The dipole between Madagascar and southern African rainfall seen in the CMIP5 climatology (Fig. 1) is similar to a well-established feature of observed rainfall variability (e.g., Jury 1992; Washington 1999; Mutai et al. 1998). Wet years in subtropical southern Africa are usually accompanied by relatively dry years over



northern Madagascar and are associated with anomalous penetration of the cross-equatorial northeasterly flow into the Kalahari basin (e.g., Hachigonta and Reason 2006; Washington and Preston 2006). Meanwhile, wet years in northern Madagascar are associated with a strengthening of the monsoonal northwesterlies toward northern Madagascar, and low geopotential heights in the southwestern Indian Ocean (Fauchereau et al. 2009; Jury 2016). In southern Madagascar, rainfall tends to vary in phase with rainfall over southern Africa (e.g., Fauchereau et al. 2009; Randriamahefasoa and Reason 2017). With this in mind, we now evaluate differences in the mean circulation among CMIP5 models.

#### 4. CMIP5 circulation

##### a. Zonal overturning circulation

We start our analysis of the CMIP5 models by examining the climatological zonal overturning circulation for 10°–70°E averaged over 23°–30°S during January–February (Fig. 3). At 20°–30°E in reanalysis data (top left), there is shallow overturning circulation comprising dry convection associated with the Kalahari heat low (20°–30°E) and subsidence in eastern southern Africa and the Mozambican channel. Farther east, over Madagascar (50°E), deeper convection, up to 200 hPa, is coupled with the south Indian Ocean high (SIOH) and is part of the canonical Walker circulation.

The CMIP5 ensemble does not reproduce this circulation. Most models, especially at the wetter end of the spectrum, simulate convection that is too deep over the subcontinent where the shallow Kalahari heat low is present in reality. Meanwhile, more than half of the models (11/19) fail to simulate convection over Madagascar. This is consistent with the dipole rainfall bias among most models (Fig. 1). Of the models that do simulate convection over Madagascar, only five show it as separate from subcontinental convection. One consequence of these errors is that the majority of models simulate a single overturning cell that links deep convection over land to subsidence over the south Indian Ocean. This is in contrast to the two-cell system seen in both ERA-Interim and NCEP2.

To explore the deep convection bias in more detail we compare the vertical structure of moist static energy (MSE) in models with radiosonde data at Upington (28.24°S, 21.16°E). Moist static energy is defined as

$$\text{MSE} = C_p T + gz + Lq. \quad (1)$$

The first two terms on the right-hand side represent the dry static energy (DSE) contribution;  $C_p T$  is the sensible heat, and  $gz$  is potential energy. The last term is the latent

heat component;  $L$  is the latent heat of condensation, and  $q$  is the specific humidity. For most models (solid lines), the vertical gradient in MSE between the surface and 700 hPa is too steep (Fig. 4a) and ~75% of the models (16/22) simulate excessive surface MSE on the order of 5–10 kJ kg<sup>−1</sup> compared to the radiosonde estimate (dashed lines). ERA-Interim and NCEP2 (dotted lines) also have a positive MSE bias compared to the radiosonde data, although the MSE gradient is better reproduced.

There is an opposite sign of model bias in the two components of MSE: the dry static energy component of MSE is underestimated in all models (Fig. 4b) while specific humidity is overestimated in all but one model (GISS-E2-R). At 800 hPa, the simulated specific humidity exceeds the radiosonde estimate by between 25% and 90% in 16 of 22 models (Fig. 4c). The excessive moisture decreases the minimum dewpoint depression (the difference between the temperature and dewpoint temperature) in models (Fig. 4d). Over half the models simulate a mean dewpoint depression at 700 hPa of between 6 and 11 K, whereas in the radiosonde estimate the range in dewpoint depression between night and day is between 11 and 19 K. This suggests that convection is much more likely in models compared to reality, consistent with Fig. 3.

The biases compared to radiosonde data in Pretoria (26°S, 28°E) at an elevation of 1526 m are more complex than at Upington (not shown). In Pretoria, there is a tendency to underestimate specific humidity near the surface but to overestimate specific humidity above 700 hPa. The overestimation of specific humidity at lower to middle levels in the atmosphere, coupled with an underestimation of dry static energy, results in an overall low bias in the dewpoint depression, which is especially prominent with respect to the daytime (1200 UTC) radiosonde profile. Interestingly, the profile at 0200 LT shows that the dewpoint depression near the surface at 850 hPa is low (2–3 K), consistent with frequent dew formation previously reported by (Nagel 1962). The mean temperature profile at 0200 LT is almost isothermal in the boundary layer, suggesting efficient longwave cooling over the high plateau.

There is some uncertainty in comparing model grids (at 2° × 2°) with a point observation, particularly as we only have a relatively short record available from the Upington radiosonde station (see section 2). However, our results are in agreement with previous work that highlights the CMIP5 cool temperature bias and excessive specific humidity in southern Africa (Flato et al. 2013; Mueller and Seneviratne 2014). Since excessive specific humidity appears to be linked to the enhanced MSE, and by extension convection, our challenge now is to work out why there is excessive moisture in models compared to reality.

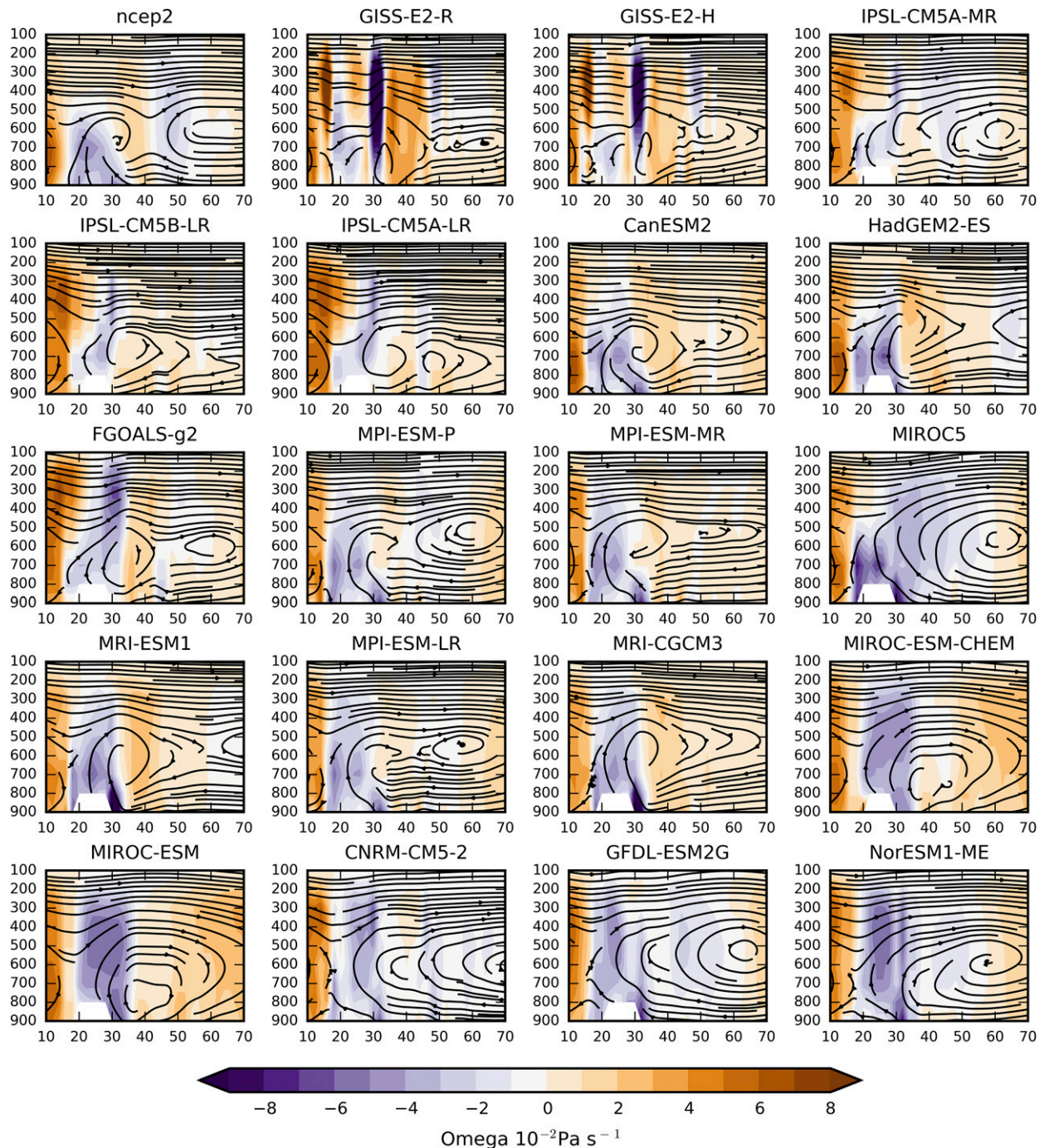


FIG. 3. Longitude ( $^{\circ}$ E)–height (hPa) cross sections of streamlines ( $u, w \times 10^2$ ) averaged over  $23^{\circ}$ – $29^{\circ}$ S in (top left) NCEP2 and CMIP5 models ordered from dry to wet (Table 1). Shading is vertical velocity ( $\text{Pa s}^{-1} \times 10^2$ ), with purple shades as negative (upward) vertical velocity and orange shades as positive (downward) vertical velocity. ERA-Interim is not included here but is qualitatively similar to NCEP2. HadGEM2-CC, MIROC4h, and CNRM-CM5 did not have vertical velocity data available and are not included.

#### b. Moisture circulation in wet and dry models

We investigate the proximate causes of excessive moisture in models over the interior of subtropical

southern Africa by examining the differences in low-level (850 hPa) moisture circulation between dry and wet models (Fig. 5). In wet models, moisture penetrates farther into the subtropics from the northeast, and over



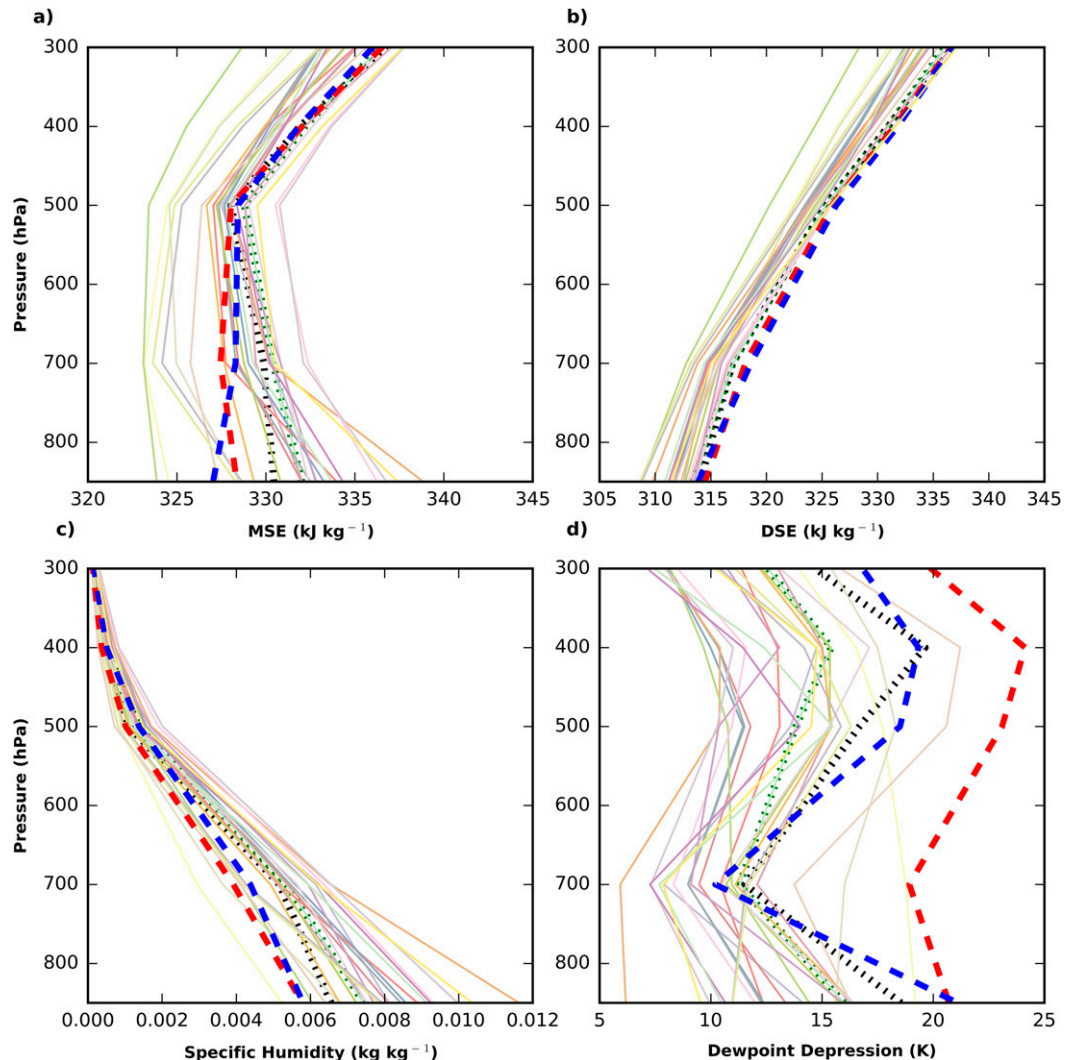


FIG. 4. JF climatological vertical profiles of (a) MSE, (b) DSE, (c) specific humidity, and (d) dewpoint depression at Upton (28°S, 21°E). The red and blue dashed lines are the average of 1400 and 0200 LT radiosonde data, respectively. The solid lines are estimates of the daily mean vertical profile from CMIP5 models; the green (black) dotted lines are for the ERA-Interim (NCEP2) reanalysis. For reanalyses and models we have used data from the grid box closest to the Upton station.

the Tanzanian Escarpment, resulting in anomalous northeasterly flow across Zimbabwe and Botswana on the order of  $10\text{--}30 \text{ g kg}^{-1} \text{ ms}^{-1}$ . This corresponds to enhanced MSE at 850 hPa of up to  $9 \text{ kJ kg}^{-1}$  in the Kalahari region (Fig. 5c). The northeasterly moisture flux occurs in preference to the southeasterly recurvature of the monsoonal northeasterlies out toward the south Indian Ocean. As a consequence, south of  $10^\circ\text{S}$  there is almost no westerly moisture flow out into the subtropical Indian Ocean in wet models.

In dry models there is little penetration of moisture across the Tanzanian–Zambian border and some of the northeasterly flow slows and curves southeastward toward Madagascar. This prevents the penetration of

easterly flow across the north of Madagascar and is associated with higher MSE (by  $5 \text{ kJ kg}^{-1}$ ) in the south Indian Ocean in the dry set of models. Differences in dry static energy between wet and dry models are negligible (not shown), emphasizing the central role played by the provision of water vapor. The preferential supply of moisture into the subcontinent rather than into the southwestern Indian Ocean in wetter models could therefore be the leading contributor to the dipole precipitation bias (Fig. 1).

We cannot demonstrate cause and effect in the context of the CMIP5 ensemble, as the relationship between convection and water vapor provision is two-way: convection moistens the troposphere and the diabatic

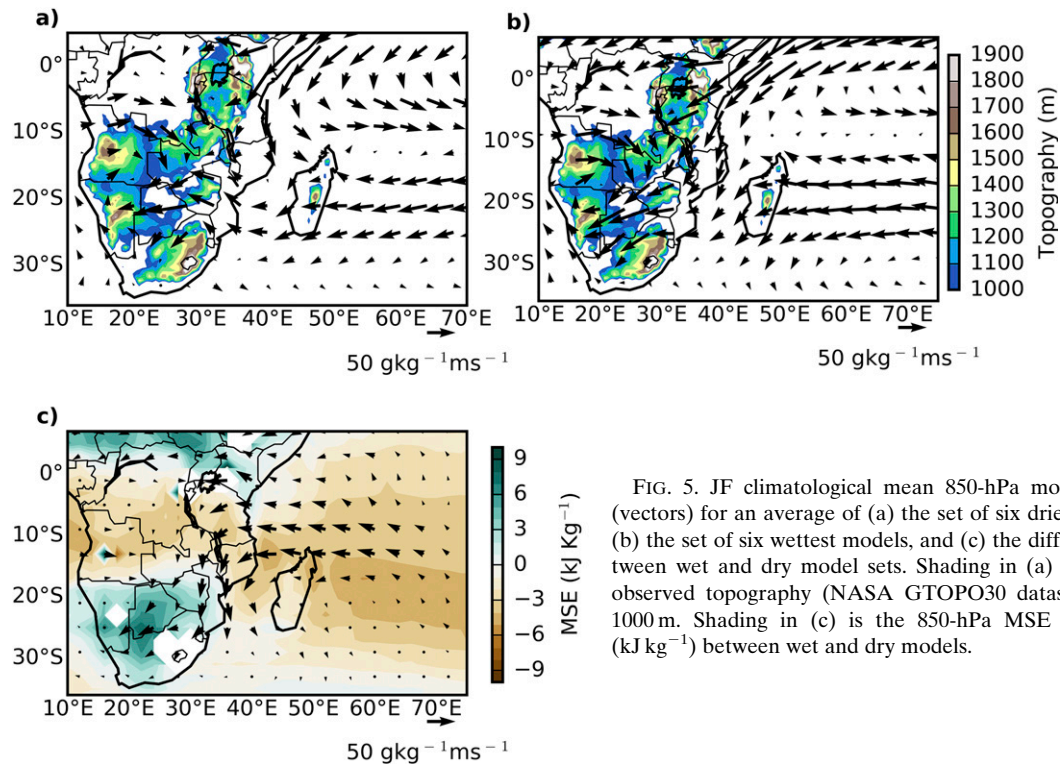


FIG. 5. JF climatological mean 850-hPa moisture flux (vectors) for an average of (a) the set of six driest models, (b) the set of six wettest models, and (c) the difference between wet and dry model sets. Shading in (a) and (b) is observed topography (NASA GTOPO30 dataset) above 1000 m. Shading in (c) is the 850-hPa MSE difference ( $\text{kJ kg}^{-1}$ ) between wet and dry models.

heating associated with convection enhances the large-scale moisture inflow. Instead, our aim for the next section is to diagnose the link between the northeasterly flow and model rainfall.

### c. Upstream circulation, topography, and CMIP5 rainfall

#### 1) FROUDE NUMBER IN CMIP5 MODELS

To reach the Kalahari basin, the northeasterly moisture flow must overcome the barrier of the Tanzanian Escarpment. In the previous section we saw that this occurs in wet models but not in dry models or in reanalyses. As rotational effects are weak owing to the low latitude, the ability of the flow to pass over a barrier is primarily dependent on the balance of inertial and gravitational forces and can be estimated using the nondimensional mountain Froude number ( $\text{Fn}$ ):

$$\text{Fn} = \frac{U}{Nh}, \quad (2)$$

where  $U$  is the mean wind velocity associated with upstream northeasterly flow at 850 hPa (averaged over  $36^{\circ}$ – $42^{\circ}\text{E}$ ,  $3^{\circ}$ – $11^{\circ}\text{S}$ ), and  $N$  is the moist Brünt-Väisälä frequency. The mean height  $h$  of the modeled topography is that oriented perpendicular to the northeasterly flow ( $30^{\circ}$ – $34^{\circ}\text{E}$ ,  $5^{\circ}$ – $13^{\circ}\text{S}$ ; also shown in the box in

Fig. 7). When upstream flow is strong and stability weak,  $\text{Fn}$  is relatively large and the depth of blocked flow is small. Conversely with relatively weak flow and strong stability,  $\text{Fn}$  is small and the blocking height is large. In this case, flow would be diverted around the barrier.

If blocking of the northeasterly flow is important for model rainfall variability, we would expect dry models over southern Africa to have a lower Froude number than wet models. Figure 6 demonstrates that this is the case; there is a strong positive correlation between model Froude number and precipitation over the Kalahari basin ( $r = 0.85$ ;  $p < 0.0001$ ). Models with a high Froude number, indicative of a reduced tendency to block the northeasterly flow, tend to be wetter. The slope of the regression is steep: every increase of 0.1 in Froude number corresponds to a  $1.6 \text{ mm day}^{-1}$  increase in the simulated rainfall among models. The reanalysis data (diamonds in Fig. 6) agree with drier models in the ensemble in estimating relatively low Froude numbers (0.27–0.33). The only two models (GISS-E2-H and GISS-E2-R) that simulate lower Froude numbers than the reanalysis (NCEP2) are also the only two models with the opposite sign of rainfall dipole bias (dry southern Africa, wet Madagascar). This suggests that the Froude number is an effective diagnostic for southern African rainfall simulations.



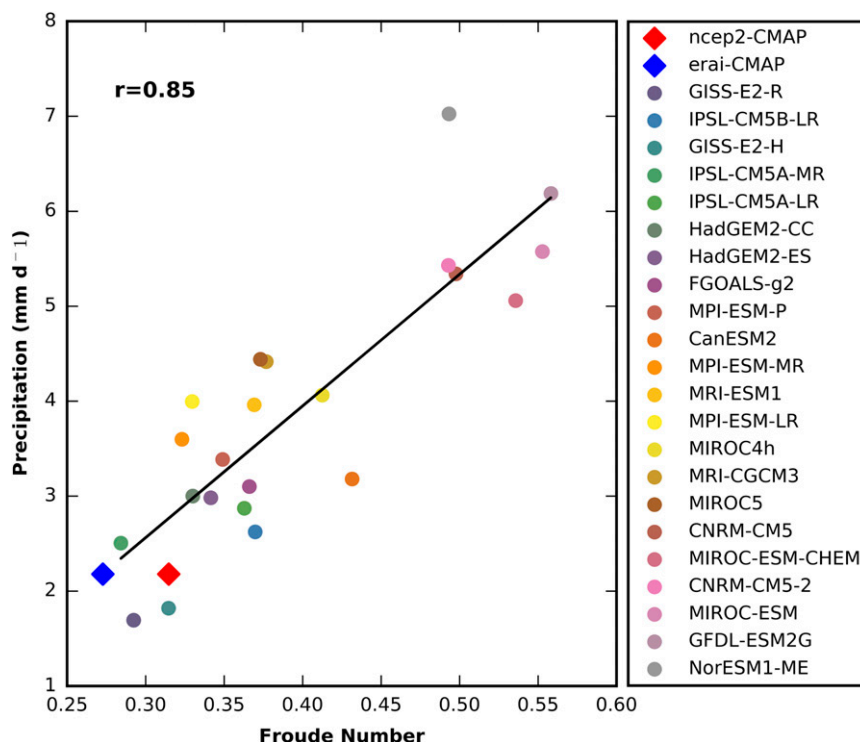


FIG. 6. The relationship between JF climatological (1979–2005) model Froude number (details in text) and mean subtropical southern Africa precipitation ( $20^{\circ}$ – $30^{\circ}$ E,  $20^{\circ}$ – $30^{\circ}$ S). Diamonds represent reanalyses and satellite-rain gauge estimates.

The spatial correlation between the simulated Froude number and gridbox rainfall across models (Fig. 7) provides support for our hypothesis that differences in the representation of the northeasterly flow are closely related to the dipole rainfall bias. After controlling for spurious gridpoint significance due to multiple hypothesis testing following Wilks (2016), we find that strong positive correlations in the Kalahari region are accompanied by a region of strong negative correlations in the southwestern Indian Ocean, to the east of Madagascar. Here, models with a greater tendency to block the northeasterly flow (lower Froude number) simulate more rainfall. This is consistent with composites of moisture flux (Fig. 5), which show the southeastward recurvature and convergence of northeasterly flow to the north and east of Madagascar in the dry set of models.

## 2) COMPONENTS OF THE FROUDE NUMBER

The intermodel spread in simulated Froude number contains contributions from the different terms  $U$ ,  $N$ , and  $h$ . The relative importance of these contributions can be estimated by calculating their coefficient of variation (multimodel mean divided by intermodel standard deviation). The intermodel coefficient of variation is 17%, 9% and 2% for  $U$ ,  $N$ , and  $h$ , respectively. This

implies that differences in model circulation, and especially in upstream wind speed, are particularly important for model variability in Froude number and rainfall. In the following we discuss the model biases for each component in turn, with the aim of making the potential future model improvements more tractable.

### (i) Static stability

There is no relationship between the model variability in the simulated moist Brünt–Väisälä frequency and precipitation in southern Africa (not shown). The moist Brünt–Väisälä frequency in 14 out of 22 models falls within the range of the NCEP2 and ERA-Interim estimates. This suggests that the upstream wind speed or topography, or a combination of the two, is responsible for the high simulated Froude numbers and penetration of moisture over the Tanzanian topography. The differences in static stability are, however, relatively large and do modulate the relationship between Froude number and precipitation.

### (ii) Upstream wind speed

Figure 8 shows that the differences among models in wind speed upstream of the Tanzanian domain are large,

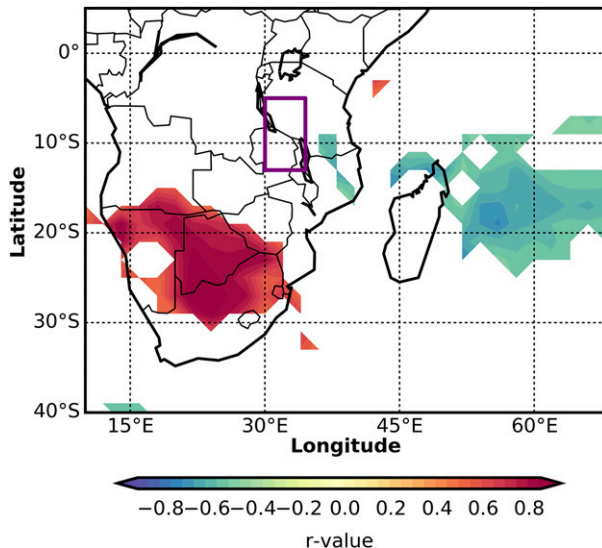


FIG. 7. Pearson's correlation coefficients for the relationship between JF climatological (1979–2005) model Froude number (details in text) and gridded rainfall over southern Africa. We control for the false discovery rate (FDR) of significant correlation following Wilks (2016), with a conservative control FDR value of  $\alpha_{\text{FDR}} = 0.10$  yielding a threshold level of significance as  $p_{\text{FDR}} = 0.026$ . Nonsignificant values are masked. The purple box shows the Tanzanian Escarpment region.

and mostly overestimated in models compared to reanalyses. In the wettest models, the northeasterly flow is  $2\text{--}3\text{ m s}^{-1}$  faster than reanalysis and only one model (GISS-E2-R) simulates slower wind speeds than the reanalyses. Conspicuously, the GISS-E2-R model is the only one of two models with rainfall dipole of opposite sign (dry southern Africa, wet Madagascar). The systematic overestimation of the strength of the northeasterlies has serious implications for cross-equatorial mass flux. For example, in the boreal summer the reversed jet (Findlater jet), which is of similar magnitude to the jet in wet models during austral summer ( $\sim 7\text{ m s}^{-1}$ ), is responsible for roughly half the global atmospheric cross-equatorial mass flux (Findlater 1969).

While rotational effects are likely to be weak owing to the low latitude, we note here that the intensified upstream wind speed will tend to increase the Rossby number (Ro) in models:

$$\text{Ro} = \frac{U}{Lf}, \quad (3)$$

where  $L$  is length scale of cross equatorial flow of magnitude  $10^6\text{ m}$ , and  $f$  is the Coriolis frequency. The Rossby number varies between models from 0.25 to 0.5 with increasing wind speed (as  $L$  and  $f$  are approximately constant between models). The relatively low Rossby number (lower wind speed) in dry models

compared to wet models implies a greater role for rotational effects, which could encourage the eastward deflection of the flow toward Madagascar. Rotational effects are less important in wet models with higher Rossby numbers.

### (iii) Topography

Although the circulation components dominate the model variability in Froude number, the model representation of topography could also be important. Figure 9 shows the longitudinal cross section of surface height at  $10^\circ\text{S}$  across the African continent ( $10^\circ\text{--}45^\circ\text{E}$ ) for CMIP5 models compared to the observed height as estimated by a global digital elevation model (GTOPO30) at  $1/6^\circ$  resolution. In the Tanzanian Escarpment region ( $30^\circ\text{--}36^\circ\text{E}$ ), limits on model resolution result in a lower, smoother barrier to the northeasterly flow. At some longitudes (e.g.,  $35^\circ\text{E}$ ), the resolved topography in the median model is a third of the height of the observed topography ( $\sim 600\text{-m}$  difference) and all models produce just one peak in topography associated with the Tanzanian Escarpment, whereas there are four peaks in reality.

The lower and smoother barrier is likely to be less effective in blocking the northeasterly flow. Figure 10 shows that models with lower resolved topography in the Tanzanian Escarpment region ( $30^\circ\text{--}36^\circ\text{E}$ ,  $5^\circ\text{--}13^\circ\text{S}$ ) tend to simulate greater downstream ( $20^\circ\text{--}42^\circ\text{E}$ ,  $20^\circ\text{--}30^\circ\text{S}$ ) northeasterly flow ( $r = -0.65$ ,  $p = 0.001$ ) and more rainfall in the Kalahari basin ( $r = -0.59$ ,  $p = 0.004$ ). The difference in rainfall between an average of six models with the highest and lowest topography over the Tanzanian Escarpment supports this result (Fig. 11). Models with low topography tend to simulate more rainfall over subtropical southern Africa and less rainfall over northern Madagascar. Improving the resolved topography may, therefore, improve the model simulation of climatological rainfall over southern Africa.

Given the large differences between the observed and simulated topography, the intermodel spread in the magnitude of low-level blocking will also depend on how unresolved orographic drag effects are represented in parameterization schemes (Lott and Miller 1997). Such schemes are only implemented in some CMIP5 models (Pithan et al. 2016) and yet have been shown to dramatically alter circulation and precipitation on a global scale (e.g., Pithan et al. 2016; van Niekerk et al. 2016). In southern Africa, the influence of model topography parameterizations is not known, although model experiments have demonstrated that the regional topography can influence key climatic features, including the cross-equatorial northeasterly flow (Slingo et al. 2005) and the cold sea surface

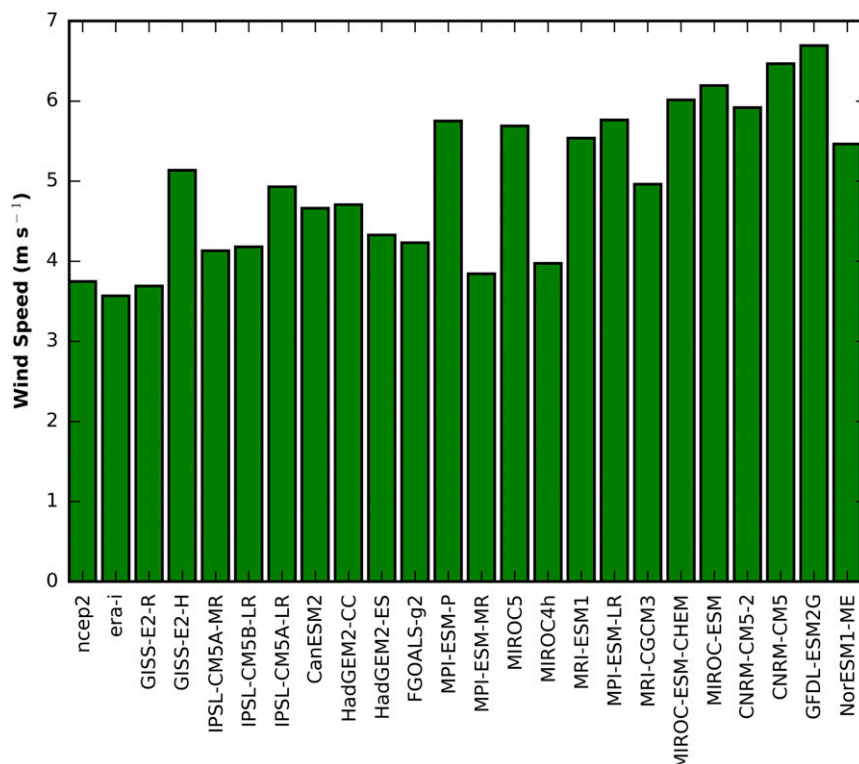


FIG. 8. Wind speed ( $\text{m s}^{-1}$ ) upstream of Tanzania at  $36^{\circ}$ – $42^{\circ}\text{E}$ ,  $3^{\circ}$ – $11^{\circ}\text{S}$  in reanalyses (first two bars) and CMIP5 models (ordered from dry to wet; see Table 1).

temperature (SST) of the Benguela upwelling zone (Potter et al. 2017).

## 5. Summary and discussion

### a. Summary of the processes associated with intermodel rainfall variability

CMIP5 models simulate too much summer rainfall over southern Africa, but too little over Madagascar. This paper shows that the dipole bias is related to some fundamental errors in the modeled regional circulation. Most models simulate the ascending branch of subtropical Walker circulation over the subcontinent, whereas in reanalyses the main region of ascent is over Madagascar (Fig. 3). As a consequence, most models simulate just one single overturning cell that links convection over southern Africa with subsidence over the Indian Ocean. The observed picture is more complicated, with shallow convection associated with the Kalahari heat low comprising one part of a two-cell overturning system in the subtropical southern Africa–Indian Ocean sector (Fig. 3). The presence of this two-cell Walker circulation over southern Africa can also be inferred from Schwendike et al. (2014) (their Fig. 2).

The wettest models over southern Africa simulate an enhanced northeasterly moisture flux that penetrates

across the high topography of Malawi and Tanzania and into the Kalahari basin. In dry models and in reanalysis the northeasterly flux curves to the southeast in the vicinity of this topography and toward the convective center over Madagascar. The model variation in simulated Froude number, a measure of the flow's ability to pass over the Tanzanian topography, is strongly associated with intermodel rainfall variability over southern Africa ( $r = 0.85$ ,  $p < 0.0001$ ). Models with reduced tendency to block the oncoming northeasterly flow simulate more rainfall over southern Africa. This is accompanied by a reduction in rainfall over southwestern Indian Ocean in those models with a higher Froude number. The model biases in the northeasterly moisture flow are similar to the anomalies observed during wet years in the interannual record (e.g., Washington and Preston 2006).

In subtropical southern Africa, a high proportion of summer rainfall falls during infrequent weather events including tropical–temperate cloud bands (Harrison 1984; Hart et al. 2013), cutoff lows (Favre et al. 2013), mesoscale convective complexes (Blamey and Reason 2013), and tropical lows (Mudenda and Mumba 1996; Reason and Keibel 2004; Howard and Washington 2018). The CMIP5 biases in the mean climatology might



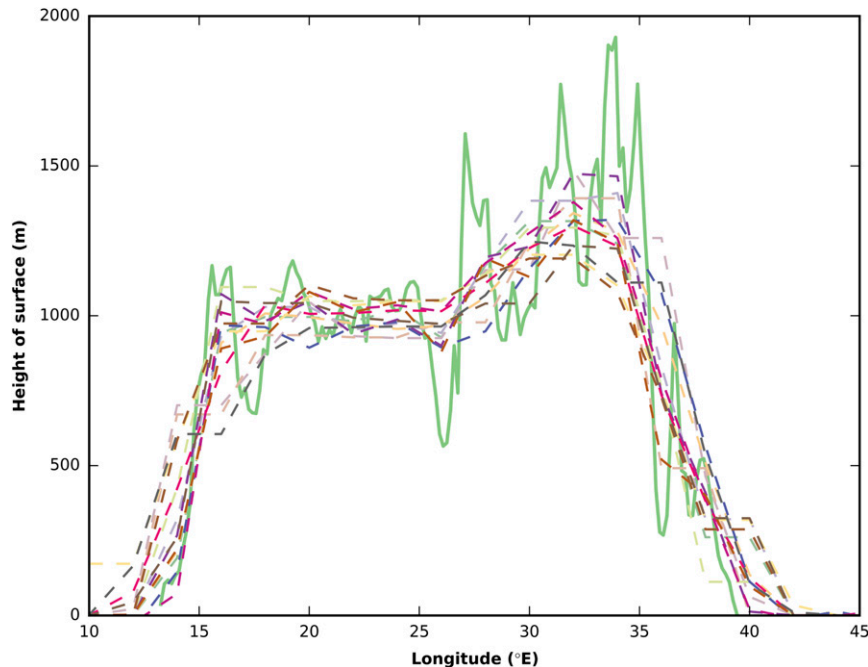


FIG. 9. Longitudinal cross section of surface height across southern Africa at 10°S for CMIP5 models (dotted lines) and NASA GTOPO30 (green solid line).

influence, or be influenced by, their simulation of these weather events although this has not yet been investigated in any depth. One exception is a study by James et al. (2018), who find that the seasonal cycle of tropical temperate cloud bands (TTCBs) is misrepresented in a recent version of the Met Office Unified Model (HadGEM3-GC2). The model simulates too many cloud bands in winter and too few in the summer, and there is too much rainfall associated with TTCBs in December. Understanding why this occurs, and whether it is a common bias across models, is a logical next step from the present study and may give further insights into the mean state biases we have investigated here.

#### *b. Foci for model development*

Our results highlight two foci for model development that may improve the simulation of southern African summer rainfall among climate models. The first is the model representation of the cross-equatorial northeasterly flow. Most models overestimate the strength of the flow compared to reanalyses (by over 50% in some cases) and the variation in its strength among models is linked with intermodel rainfall variability both in southern Africa and the southwestern Indian Ocean. The link between southern African precipitation and cross-equatorial moisture transport is consistent with model experiments that have shown that the accurate representation of cross-equatorial energy transport

improves representation of precipitation both globally and in southern Africa (Hwang and Frierson 2013; Hawcroft et al. 2017). Understanding what drives the bias in northeasterly flow should be a priority.

Previous work on southern African rainfall biases in climate models also highlights the importance of understanding causes of climate model differences in low-level moisture circulation (Moufouma-Okia and Jones 2015; Lazenby et al. 2016; Munday and Washington 2017). Moufouma-Okia and Jones (2015) show in an atmosphere-only model that errors in simulated vertically integrated moisture flux in southern Africa are correlated with errors in rainfall over the period 1980–2008. Munday and Washington (2017), meanwhile, show that some of the CMIP5 intermodel variability in low-level moisture flux and rainfall in tropical and eastern southern Africa is related to the strength of the Angola low pressure system.

Our results demonstrate a link between the mean height of resolved topography in the Tanzania–Malawi region and rainfall over southern Africa ( $r = -0.59$ ,  $p = 0.004$ ). Models with lower topography tend to simulate faster downstream northeasterly flow and more rainfall compared to those with high topography. This implies that improving model representation of topography either through increased model resolution or improved parameterizations of topographic effects could improve model rainfall, a claim that is consistent with a number of studies using both regional and global climate models

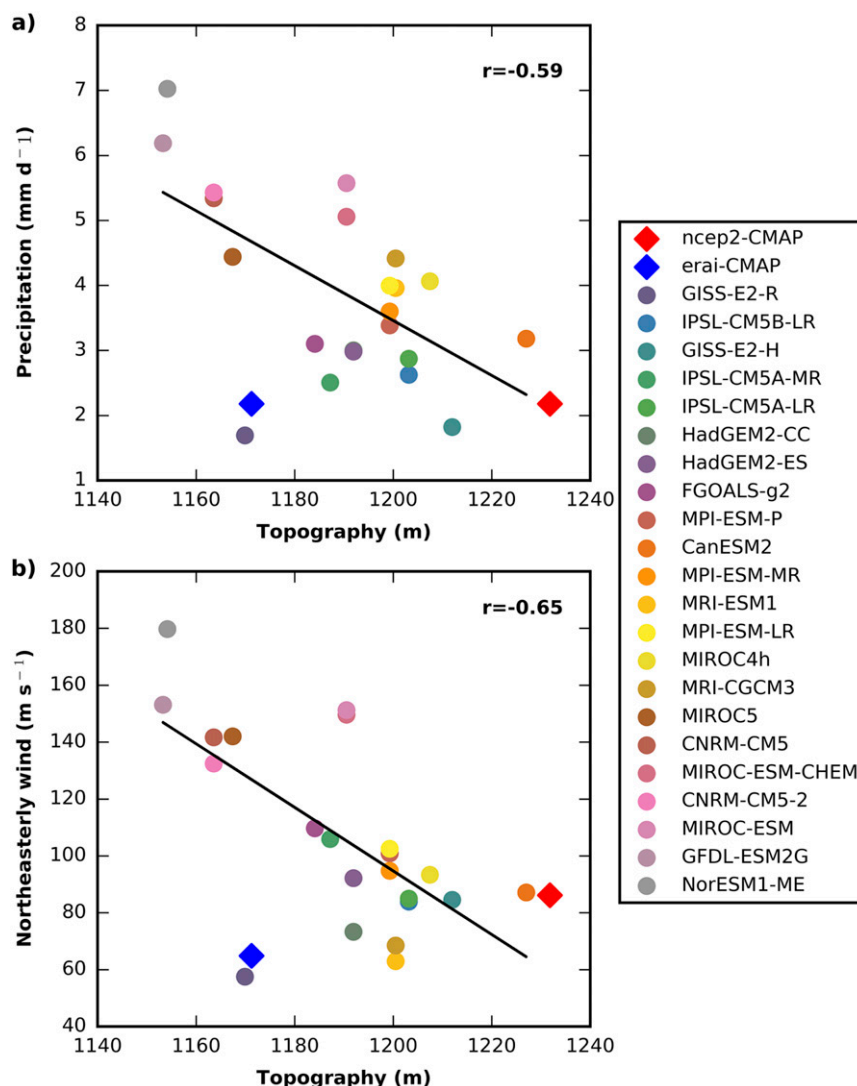


FIG. 10. The relationship between the Tanzanian Escarpment topography ( $5^{\circ}$ – $13^{\circ}\text{S}$ ,  $30^{\circ}$ – $36^{\circ}\text{E}$ ) and (a) Kalahari basin precipitation ( $20^{\circ}$ – $30^{\circ}\text{E}$ ,  $20^{\circ}$ – $30^{\circ}\text{S}$ ), and (b) total downstream wind speed (850 hPa) in a northeasterly direction ( $20^{\circ}$ – $42^{\circ}\text{E}$ ,  $20^{\circ}$ – $30^{\circ}\text{S}$ ). To compute total downstream northeasterly flow we mask grid boxes with westerly and southerly flow, compute wind speed at remaining grid boxes, and sum the wind speed across these grid boxes.

(Mason and Joubert 1997; Mehran et al. 2014; Favre et al. 2016; Pinto et al. 2016).

## 6. Conclusions

The organization of the mean regional circulation over subtropical southern Africa is fundamentally different in a majority of CMIP5 models compared to reanalyses. When these models are used to simulate future climate, a climate forcing is imposed on a mean state that is not observed. Evaluating the uncertainty in the climate change signal from this background state is therefore difficult, especially since we do not know

ahead of time whether or how the present-day bias might influence the response to forcing. It will be interesting to investigate whether the models analyzed here that do simulate a reasonable precipitation and circulation climatology (GISS-E2-H, GISS-E2-R, and IPSL-CM5A-MR) project a distinct climate change response in southern Africa compared to other models in the ensemble. This is the subject of our current work.

In addition to highlighting the potential importance of the cross-equatorial northeasterly flow and of topography for model rainfall biases, the analysis of the CMIP5 ensemble raises interesting questions about how the southern African climate system works in reality.

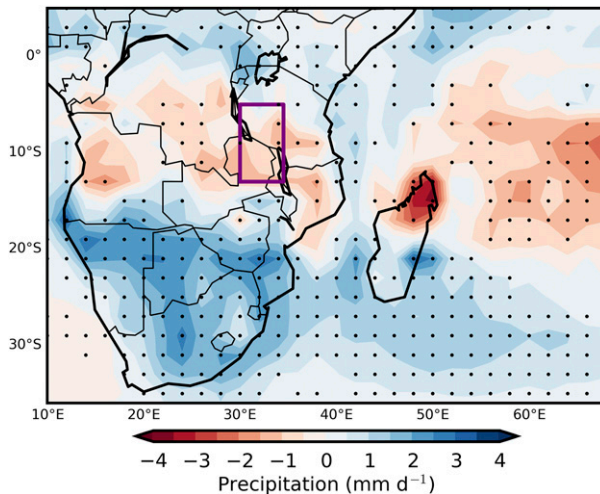


FIG. 11. The difference in climatological JF rainfall between the six models with the lowest average topography and the six models with the highest average topography over the Tanzanian Escarpment (purple box). Stipples indicate grid boxes where at least 5 out of 6 models with low topography over the Tanzanian escarpment are wetter (blues) or drier (reds) than all of the models with relatively high topography.

Among models, there is a trade-off between moisture supply to the continent and into the southwestern Indian Ocean (Fig. 5). In the present day, most models tend to supply too much moisture into the subcontinent and this is tightly coupled with an increase in subcontinental convection at the expense of precipitation over northern Madagascar. The observed balance of moisture supply in favor of northern Madagascar may contribute to its relative wetness compared to subtropical southern Africa at the same latitudes.

**Acknowledgments.** The first author is funded by the U.K. Natural Environmental Research Council (NERC) through the doctoral training partnership (NE/L002612/1) and also through a Met Office CASE studentship (ACR00400). Richard Washington is partially supported by the NERC-DfID funded UMFULA (NE/M020207/1) and IMPALA (NE/M017206) African climate programs. The climate model data are downloaded from the Earth System Grid Federation (ESGF) (<https://pcmdi.llnl.gov/>). NCEP2, ERA-Interim, and CMAP data were sourced from NOAA/OAR/ESRL PSD, Boulder, Colorado, at <http://www.esrl.noaa.gov/psd/>. Radiosonde data from Upington are available from the Integrated Global Radiosonde Archive (IGRA) (<https://www.ncdc.noaa.gov/data-access/weather-balloon/integrated-global-radiosonde-archive>) and the USGS GTOPO30 global digital elevation model data from <http://earthexplorer.usgs.gov/>. In addition to three

reviewers, whose comments improved the manuscript, we thank members of the SOGE climate lab and Annelize van Niekerk for useful discussions.

## REFERENCES

- Awange, J. L., V. G. Ferreira, E. Forootan, Khandu, S. A. Andam-Akorful, N. O. Agutu, and X. F. He, 2015: Uncertainties in remotely sensed precipitation data over Africa. *Int. J. Climatol.*, **36**, 303–323, <https://doi.org/10.1002/joc.4346>.
- Biasutti, M., 2013: Forced Sahel rainfall trends in the CMIP5 archive. *J. Geophys. Res. Atmos.*, **118**, 1613–1623, <https://doi.org/10.1002/jgrd.50206>.
- Blamey, R. C., and C. J. C. Reason, 2013: The role of mesoscale convective complexes in southern Africa summer rainfall. *J. Climate*, **26**, 1654–1668, <https://doi.org/10.1175/JCLI-D-12-00239.1>.
- Chan, S. C., and S. Nigam, 2009: Residual diagnosis of diabatic heating from ERA-40 and NCEP reanalyses: Intercomparisons with TRMM. *J. Climate*, **22**, 414–428, <https://doi.org/10.1175/2008JCLI2417.1>.
- Christensen, J. H., and Coauthors, 2007: Regional climate projections. *Climate Change 2007: The Physical Science Basis*, S. Solomon et al., Eds., Cambridge University Press, 847–940.
- Cook, K. H., 2000: The South Indian convergence zone and interannual rainfall variability over southern Africa. *J. Climate*, **13**, 3789–3804, [https://doi.org/10.1175/1520-0442\(2000\)013<3789:TSICZA>2.0.CO;2](https://doi.org/10.1175/1520-0442(2000)013<3789:TSICZA>2.0.CO;2).
- D'Abreton, P. C., and P. D. Tyson, 1995: Divergent and non-divergent water vapour transport over southern Africa during wet and dry conditions. *Meteor. Atmos. Phys.*, **55**, 47–59, <https://doi.org/10.1007/BF01029601>.
- Dee, D. P., and Coauthors, 2011: The ERA-Interim reanalysis: Configuration and performance of the data assimilation system. *Quart. J. Roy. Meteor. Soc.*, **137**, 553–597, <https://doi.org/10.1002/qj.828>.
- Dieppois, B., M. Rouault, and M. New, 2015: The impact of ENSO on Southern African rainfall in CMIP5 ocean atmosphere coupled climate models. *Climate Dyn.*, **45**, 2425–2442, <https://doi.org/10.1007/s00382-015-2480-x>.
- Fauchereau, N., B. Pohl, C. J. C. Reason, M. Rouault, and Y. Richard, 2009: Recurrent daily OLR patterns in the southern Africa/southwest Indian ocean region, implications for South African rainfall and teleconnections. *Climate Dyn.*, **32**, 575–591, <https://doi.org/10.1007/s00382-008-0426-2>.
- Favre, A., B. Hewitson, C. Lennard, R. Cerezo-Mota, and M. Tadross, 2013: Cut-off lows in the South Africa region and their contribution to precipitation. *Climate Dyn.*, **41**, 2331–2351, <https://doi.org/10.1007/s00382-012-1579-6>.
- , and Coauthors, 2016: Spatial distribution of precipitation annual cycles over South Africa in 10 CORDEX regional climate model present-day simulations. *Climate Dyn.*, **46**, 1799–1818, <https://doi.org/10.1007/s00382-015-2677-z>.
- Findlater, J., 1969: A major low-level air current near the Indian Ocean during the northern summer. *Quart. J. Roy. Meteor. Soc.*, **95**, 362–380, <https://doi.org/10.1002/qj.49709540409>.
- Flato, G., and Coauthors, 2013: Evaluation of climate models. *Climate Change 2013: Physical Science Basis*, T. F. Stocker et al., Eds., Cambridge University Press, 741–866, <https://doi.org/10.1017/CBO9781107415324>.
- Goddard, L., and N. E. Graham, 1999: Importance of the Indian Ocean for simulating rainfall anomalies over eastern and



- southern Africa. *J. Geophys. Res.*, **104**, 19 099–19 116, <https://doi.org/10.1029/1999JD900326>.
- Hachigonta, S., and C. J. C. Reason, 2006: Interannual variability in dry and wet spell characteristics over Zambia. *Climate Res.*, **32**, 49–62, <https://doi.org/10.3354/cr032049>.
- Harrison, M. S. J., 1984: A generalized classification of South African summer rain-bearing synoptic systems. *J. Climatol.*, **4**, 547–560, <https://doi.org/10.1002/joc.3370040510>.
- Hart, N. C. G., C. J. C. Reason, and N. Fauchereau, 2013: Cloud bands over southern Africa: Seasonality, contribution to rainfall variability and modulation by the MJO. *Climate Dyn.*, **41**, 1199–1212, <https://doi.org/10.1007/s00382-012-1589-4>.
- Hawcroft, M., J. M. Haywood, M. Collins, A. Jones, A. C. Jones, and G. Stephens, 2017: Southern Ocean albedo, inter-hemispheric energy transports and the double ITCZ: Global impacts of biases in a coupled model. *Climate Dyn.*, **48**, 2279–2295, <https://doi.org/10.1007/s00382-016-3205-5>.
- Howard, E., and R. Washington, 2018: Characterizing the synoptic expression of the Angola low. *J. Climate*, <https://doi.org/10.1175/JCLI-D-18-0017.1>, in press.
- Hwang, Y.-T., and D. M. W. Frierson, 2013: Link between the double-Intertropical Convergence Zone problem and cloud biases over the Southern Ocean. *Proc. Natl. Acad. Sci. USA*, **110**, 4935–4940, <https://doi.org/10.1073/pnas.1213302110>.
- James, R., and Coauthors, 2018: Evaluating climate models with an African lens. *Bull. Amer. Meteor. Soc.*, **99**, 313–336, <https://doi.org/10.1175/BAMS-D-16-0090.1>.
- Jury, M. R., 1992: A climatic dipole governing the interannual variability of convection over the SW Indian Ocean and SE Africa region. *Trends Geophys. Res.*, **1**, 165–172.
- , 2016: Summer climate of Madagascar and monsoon pulsing of its vortex. *Meteor. Atmos. Phys.*, **128**, 117–129, <https://doi.org/10.1007/s00703-015-0401-5>.
- Kanamitsu, M., W. Ebisuzaki, J. Woollen, S.-K. Yang, J. J. Hnilo, M. Fiorino, and G. L. Potter, 2002: NCEP–DOE AMIP-II Reanalysis (R-2). *Bull. Amer. Meteor. Soc.*, **83**, 1631–1644, <https://doi.org/10.1175/BAMS-83-11-1631>.
- Lazenby, M., M. Todd, and Y. Wang, 2016: Climate model simulation of the South Indian Ocean Convergence Zone: Mean state and variability. *Climate Res.*, **68**, 59–71, <https://doi.org/10.3354/cr01382>.
- Lintner, B. R., D. K. Adams, K. A. Schiro, A. M. Stansfield, A. A. Amorim Rocha, and J. D. Neelin, 2017: Relationships among climatological vertical moisture structure, column water vapor, and precipitation over the central Amazon in observations and CMIP5 models. *Geophys. Res. Lett.*, **44**, 1981–1989, <https://doi.org/10.1002/2016GL071923>.
- Lott, F., and M. J. Miller, 1997: A new subgrid-scale orographic drag parametrization: Its formulation and testing. *Quart. J. Roy. Meteor. Soc.*, **123**, 101–127, <https://doi.org/10.1002/qj.49712353704>.
- Maidment, R. I., R. P. Allan, and E. Black, 2015: Recent observed and simulated changes in precipitation over Africa. *Geophys. Res. Lett.*, **42**, 8155–8164, <https://doi.org/10.1002/2015GL065765>.
- Manatsa, D., and C. Reason, 2017: ENSO–Kalahari Desert linkages on southern Africa summer surface air temperature variability. *Int. J. Climatol.*, **37**, 1728–1745, <https://doi.org/10.1002/joc.4806>.
- Mason, S. J., and A. M. Joubert, 1997: Simulated changes in extreme rainfall over southern Africa. *Int. J. Climatol.*, **17**, 291–301, [https://doi.org/10.1002/\(SICI\)1097-0088\(19970315\)17:3<291::AID-JOC120>3.0.CO;2-1](https://doi.org/10.1002/(SICI)1097-0088(19970315)17:3<291::AID-JOC120>3.0.CO;2-1).
- Mehran, A., A. Aghakouchak, and T. Phillips, 2014: Evaluation of CMIP5 continental precipitation simulations relative to satellite-based gauge-adjusted observations. *J. Geophys. Res. Atmos.*, **119**, 1695–1707, <https://doi.org/10.1002/2013JD021152>.
- Moise, F., and D. A. Hudson, 2008: Probabilistic predictions of climate change for Australia and southern Africa using the reliability ensemble average of IPCC CMIP3 model simulations. *J. Geophys. Res.*, **113**, D15113, <https://doi.org/10.1029/2007JD009250>.
- Moufouma-Okia, W., and R. Jones, 2015: Resolution dependence in simulating the African hydroclimate with the HadGEM3-RA regional climate model. *Climate Dyn.*, **44**, 609–632, <https://doi.org/10.1007/s00382-014-2322-2>.
- Mudenda, O. S., and Z. L. S. Mumba, 1996: The unusual tropical storm of January 1996. Zambia Meteorological Department Tech. Rep., 8 pp., [http://oiswww.eumetsat.org/WEBOPS/iotm/iotm/20100124\\_troplow/2004\\_Mudenda\\_Unusual\\_Tropical%20Storm.pdf](http://oiswww.eumetsat.org/WEBOPS/iotm/iotm/20100124_troplow/2004_Mudenda_Unusual_Tropical%20Storm.pdf).
- Mueller, B., and S. I. Seneviratne, 2014: Systematic land climate and evapotranspiration biases in CMIP5 simulations. *Geophys. Res. Lett.*, **41**, 128–134, <https://doi.org/10.1002/2013GL058055>.
- Munday, C., and R. Washington, 2017: Circulation controls on southern African precipitation in coupled models: The role of the Angola low. *J. Geophys. Res. Atmos.*, **122**, 861–877, <https://doi.org/10.1002/2016JD025736>.
- Mutai, C. C., M. N. Ward, and A. W. Colman, 1998: Towards the prediction of the East Africa short rains based on sea-surface temperature–atmosphere coupling. *Int. J. Climatol.*, **18**, 975–997, [https://doi.org/10.1002/\(SICI\)1097-0088\(199807\)18:9<975::AID-JOC259>3.0.CO;2-U](https://doi.org/10.1002/(SICI)1097-0088(199807)18:9<975::AID-JOC259>3.0.CO;2-U).
- Nagel, J. F., 1962: On the measurement of dew. *Arch. Meteor. Geophys. Bioklimat.*, **11B**, 403–423, <https://doi.org/10.1007/BF02243152>.
- Nicholson, S. E., 2018: The ITCZ and the seasonal cycle over equatorial Africa. *Bull. Amer. Meteor. Soc.*, **99**, 337–348, <https://doi.org/10.1175/BAMS-D-16-0287.1>.
- Novella, N. S., and W. M. Thiaw, 2013: African rainfall climatology version 2 for famine early warning systems. *J. Appl. Meteor. Climatol.*, **52**, 588–606, <https://doi.org/10.1175/JAMC-D-11-0238.1>.
- Pinto, I., C. Lennard, M. Tadross, B. Hewitson, A. Dosio, G. Nikulin, H. J. Panitz, and M. E. Shongwe, 2016: Evaluation and projections of extreme precipitation over southern Africa from two CORDEX models. *Climatic Change*, **135**, 655–668, <https://doi.org/10.1007/s10584-015-1573-1>.
- Pithan, F., T. G. Shepherd, G. Zappa, and I. Sandu, 2016: Climate model biases in jet streams, blocking and storm tracks resulting from missing orographic drag. *Geophys. Res. Lett.*, **43**, 7231–7240, <https://doi.org/10.1002/2016GL069551>.
- Potter, S. F., E. J. Dawson, and D. M. W. Frierson, 2017: Southern African orography impacts on low clouds and the Atlantic ITCZ in a coupled model. *Geophys. Res. Lett.*, **44**, 3283–3289, <https://doi.org/10.1002/2017GL073098>.
- Randriamahefasoa, T. S. M., and C. J. C. Reason, 2017: Interannual variability of rainfall characteristics over southwestern Madagascar. *Theor. Appl. Climatol.*, **128**, 421–437, <https://doi.org/10.1007/s00704-015-1719-0>.
- Reason, C. J. C., 2016: The Bolivian, Botswana, and Bilybara highs and Southern Hemisphere drought/floods. *Geophys. Res. Lett.*, **43**, 1280–1286, <https://doi.org/10.1002/2015GL067228>.
- , and A. Keibel, 2004: Tropical Cyclone Eline and its unusual penetration and impacts over the southern African mainland.

- Wea. Forecasting, **19**, 789–805, [https://doi.org/10.1175/1520-0434\(2004\)019<0789:TCEAIU>2.0.CO;2](https://doi.org/10.1175/1520-0434(2004)019<0789:TCEAIU>2.0.CO;2).
- Sanderson, B. M., and R. Knutti, 2012: On the interpretation of constrained climate model ensembles. *Geophys. Res. Lett.*, **39**, L16708, <https://doi.org/10.1029/2012GL052665>.
- Schwendike, J., P. Govekar, M. J. Reeder, R. Wardle, G. J. Berry, and C. Jakob, 2014: Local partitioning of the overturning circulation in the tropics and the connection to the Hadley and Walker circulations. *J. Geophys. Res. Atmos.*, **119**, 1322–1339, <https://doi.org/10.1002/2013JD020742>.
- Slingo, J., H. Spencer, B. Hoskins, P. Berrisford, and E. Black, 2005: The meteorology of the western Indian Ocean, and the influence of the East African highlands. *Philos. Trans. Roy. Soc.*, **363A**, 25–42, <https://doi.org/10.1098/rsta.2004.1473>.
- Taljaard, J. J., 1972: Synoptic meteorology of the Southern Hemisphere. *Meteorology of the Southern Hemisphere, Meteor. Monogr.*, No. 49, Amer. Meteor. Soc., 139–213.
- Taylor, K. E., R. J. Stouffer, and G. A. Meehl, 2012: An overview of CMIP5 and the experiment design. *Bull. Amer. Meteor. Soc.*, **93**, 485–498, <https://doi.org/10.1175/BAMS-D-11-00094.1>.
- Tyson, P. D., and S. J. Crimp, 1998: The climate of the Kalahari Transect. *Trans. Roy. Soc. S. Afr.*, **53**, 93–112, <https://doi.org/10.1080/00359199809520380>.
- van Heerden, J., and J. J. Taljaard, 1998: Africa and surrounding waters. *Meteorology of the Southern Hemisphere, Meteor. Monogr.*, No. 49, Amer. Meteor. Soc., 141–174.
- van Niekerk, A., T. G. Shepherd, S. B. Vosper, and S. Webster, 2016: Sensitivity of resolved and parametrized surface drag to changes in resolution and parametrization. *Quart. J. Roy. Meteor. Soc.*, **142**, 2300–2313, <https://doi.org/10.1002/qj.2821>.
- Washington, R., 1999: Interannual and interdecadal variability of African rainfall. Ph.D. thesis, University of Oxford, 258 pp.
- , and A. Preston, 2006: Extreme wet years over southern Africa: Role of Indian Ocean sea surface temperatures. *J. Geophys. Res.*, **111**, D15104, <https://doi.org/10.1029/2005JD006724>.
- Wilks, D., 2016: “The stippling shows statistically significant grid points”: How research results are routinely overstated and overinterpreted, and what to do about it. *Bull. Amer. Meteor. Soc.*, **97**, 2263–2274, <https://doi.org/10.1175/BAMS-D-15-00267.1>.
- Xie, P., and P. A. Arkin, 1997: Global precipitation: A 17-year monthly analysis based on gauge observations, satellite estimates, and numerical model outputs. *Bull. Amer. Meteor. Soc.*, **78**, 2539–2558, [https://doi.org/10.1175/1520-0477\(1997\)078<2539:GPAYMA>2.0.CO;2](https://doi.org/10.1175/1520-0477(1997)078<2539:GPAYMA>2.0.CO;2).
- Yang, W., R. Seager, M. A. Cane, and B. Lyon, 2015: The rainfall annual cycle bias over East Africa in CMIP5 coupled climate models. *J. Climate*, **28**, 9789–9802, <https://doi.org/10.1175/JCLI-D-15-0323.1>.
- Zhang, Q., H. Körnich, and K. Holmgren, 2013: How well do re-analyses represent the southern African precipitation? *Climate Dyn.*, **40**, 951–962, <https://doi.org/10.1007/s00382-012-1423-z>.